Heteronanostructures

DOI: 10.1002/anie.201101084

Matchstick-Shaped Ag_2S–ZnS Heteronanostructures Preserving both UV/Blue and Near-Infrared Photoluminescence**

*Shuling Shen, Yejun Zhang, Long Peng, Yaping Du, and Qiangbin Wang**

In recent years, heterostructured nanomaterials have attracted intense research interest due to their integrated multifunctionality of disparate components. Such multifunctionality gives heterostructured nanomaterials great potential in different fields of diagnosis, sensors, catalysis, optoelectronic devices, and so on.[1–10] In particular, enormous efforts have been devoted to synthesizing different heterodimer nanomaterials, including $CoPt_3$–Au,[3] PbSe–Au,[4] Fe_3O_4–Au,[4,5] PbS–Au,[4,6] Fe_3O_4–Ag,[7,8] and Ag_2S/Ag,[10] which combine optical and/or electrical, magnetic, catalytic properties.

Matchstick-shaped heteronanostructures (HNSs) are an important kind of heterostructured nanomaterials which are very suitable for integrating into nanodevices for further applications. Metal-tipped semiconductor nanorod HNSs have been well studied in the last decade.[11–15] Metal tips (Au, Pt, Co, etc.) were selectively grown on either top or side of CdS/CdSe nanorods, and the resulting metal–semiconductor interface facilitated charge separation,[16–18] which favored their application in solar energy. Due to the flexibility of bandgap engineering, semiconductor–semiconductor HNSs have been considered to offer better opportunities for internal exciton separation and carrier transport and optoelectronic applications.[19–22]

Recently, we reported that Ag_2S quantum dots (QDs) can be good candidates as near-infrared (NIR) emitters,[23] and that ultrathin ZnS nanowires can emit in the UV/blue region.[24] We therefore wondered how HNSs consisting of Ag_2S QDs and ZnS nanowires would behave. Recently, Xu et al. prepared Ag_2S–ZnS HNSs by a seeded-growth method in which Ag_2S nanocrystals acted as catalyst for growth of ZnS nanorods.[25] However, both Ag_2S nanocrystals and ZnS nanorods of the as-prepared Ag_2S–ZnS HNSs had large diameters of about 20 nm and their optical properties were not reported. Since the Bohr radius of ZnS is 2.4 nm (to the best of our knowledge, that of Ag_2S is unknown), we expect that Ag_2S–ZnS HNSs with smaller sizes will exhibit their intrinsic optical properties due to the quantum confinement effect. Therefore, the driving force for this work was to determine whether Ag_2S–ZnS HNSs with smaller sizes preserve both the NIR and UV/blue emissions or not. Three merits of this work can be noted: 1) The as-prepared small Ag_2S–ZnS HNSs exhibit both NIR and UV/blue emissions from Ag_2S QDs and ZnS nanorods, respectively; 2) A facile one-pot method is utilized for Ag_2S–ZnS HNSs synthesis by thermal co-decomposition of single-source precursors Ag(DDTC) and $Zn(DDTC)_2$ (DDTC = diethyldithiocarbamate), which is much more convenient than the seeded-growth or catalyst-assisted growth method; 3) The size of the HNSs can be easily tuned by changing the reaction conditions, which is not possible for seeded-growth with given seeds.

Figure 1a depicts a typical low-magnification TEM image of Ag_2S–ZnS HNSs prepared with an Ag(DDTC)/$Zn(DDTC)_2$ molar ratio of 2:1. The HNSs are of uniform matchstick shape with significant difference in the mass-thickness contrast between the spherical head (ca. 4.5 nm in diameter) and the stem (4×48 nm in diameter and length). The narrow size distribution of as-prepared Ag_2S–ZnS HNSs facilitated their self-assembly into superlattice structures with hexagonal packing, which was supported by a selected-area fast Fourier transform (FFT) pattern (inset in Figure 1a). The Ag_2S–ZnS HNS superlattices were perpendicular to the TEM grid, as was further confirmed by TEM tilting experiments (see Supporting Information), similar to a previously reported CoO nanorod superlattice.[26] The mass-thickness contrast difference between the spherical head and stem indicated the various chemical compositions of the as-prepared HNSs.

A high-resolution TEM (HRTEM) image of a typical Ag_2S–ZnS HNS is shown in Figure 1b. The HNS is highly crystalline with a spherical head and a nanorodlike stem, and has a partially coherent interface between single-crystalline head and stem. Based on the analysis of the corresponding crystal lattices, the spherical head is composed of Ag_2S and the stem of ZnS, and the conjunction interface consists of the $(\bar{1}21)$ plane of the Ag_2S head and the (008) plane of the ZnS stem with a lattice mismatch of 16% (Figure 1b). The (008) plane of ZnS was further confirmed by a higher quality HRTEM image (Figure 1c), in which hcp ABAB stacking of ZnS double layers along the [001] direction can be clearly observed. This is a strong evidence that $d = 0.31$ nm corresponds to the (008) plane of hexagonal ZnS. Detailed analysis of the local elemental composition of the Ag_2S–ZnS HNSs was performed by line-scan energy-dispersive X-ray spec-

[*] Dr. S. Shen, Y. Zhang, L. Peng, Dr. Y. Du, Prof. Dr. Q. Wang
Division of Nanobiomedicine and *i*-Lab, Suzhou Institute of Nano-Tech and Nano-Bionics, Chinese Academy of Sciences
Suzhou, 215123 (China)
Fax: (+86) 512-6287-2620
E-mail: qbwang2008@sinano.ac.cn

[**] Q.W acknowledges funding by the "Bairen Ji Hua" program "Strategic Priority Research Program" (Grant No. XDA01030200) from Chinese Academy of Sciences (CAS), MOST (Grant No. 2011CB965004), NSFC (Grant No. 20173225, 20901055), and CAS/SAFEA International Partnership Program for Creative Research Teams. The authors thank Prof. Peidong Yang at UC, Berkeley for helpful discussion. The authors express their appreciation to Electron Microscope Lab at Suzhou Institute of Nano-Tech and Nano-Bionics, CAS for the TEM facilities used in this research.

Supporting information for this article is available on the WWW under http://dx.doi.org/10.1002/anie.201101084.

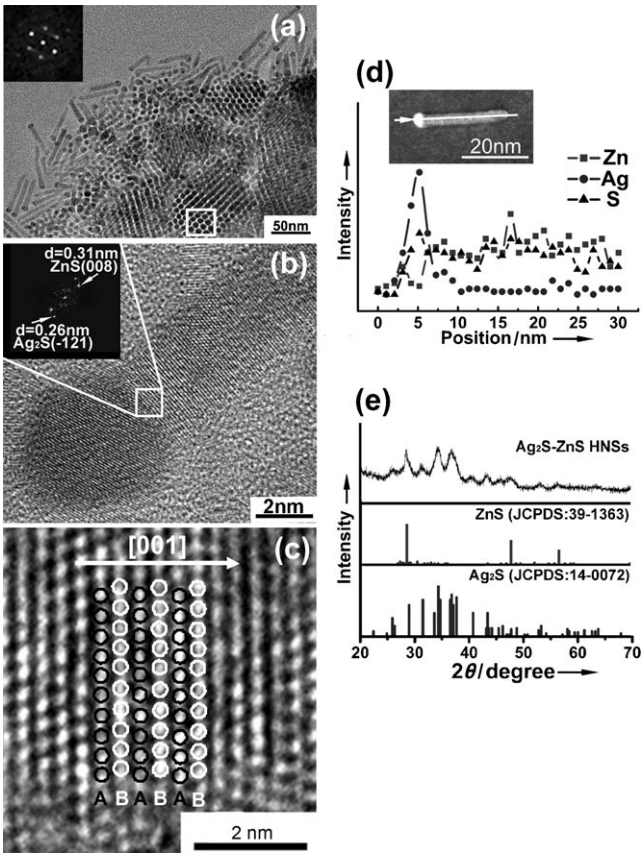

Figure 1. a) TEM image (inset: corresponding FFT pattern from a selected superlattice domain), b) HRTEM image (inset: corresponding FFT pattern from the Ag_2S–ZnS interface), and c) higher quality HRTEM image of the section of the ZnS stem of Ag_2S–ZnS HNSs. d) Elemental profiles of Ag, Zn, and S (see white line in the inset high-angle annular dark-field STEM image) and e) XRD pattern of Ag_2S–ZnS HNSs.

troscopy (Figure 1d). The elemental profiles show that Ag is limited to the head and Zn to the stem part, while sulfur is dispersed throughout the HNSs. The calculated Ag:S and Zn:S elemental ratios were close to 2:1 and 1:1, respectively, which confirms formation of Ag_2S head–ZnS stem HNSs. Although the small size of the Ag_2S–ZnS HNSs resulted in weak and broad XRD peaks (Figure 1e), monoclinic Ag_2S (JCPDS 14-0072) and hexagonal ZnS (JCPDS 39-1363) could still be clearly indexed from their characteristic Bragg peaks. No impurities were detected in our XRD measurement.

Obtaining highly crystalline Ag_2S–ZnS HNSs with well-defined features enabled further investigation of their optical properties. The Ag_2S–ZnS HNSs show both UV/blue and NIR photoluminescence (PL) with 280 and 785 nm excitation, respectively (Figure 2). In the UV/blue region, the two emission peaks at about 380 and 450 nm could be attributed to interstitial zinc (shallow-acceptor emission) and deep-trap emission arising from surface vacant sulfur sites of ZnS, respectively.[27,28] In comparison with the reported PL spectrum of ZnS nanowires,[24,27] the emission at about 358 nm originating from interstitial sulfur is eclipsed in the Ag_2S–ZnS HNSs, and this may be ascribable to coupling between ZnS nanorods and Ag_2S QDs.[21] A symmetric emission peak

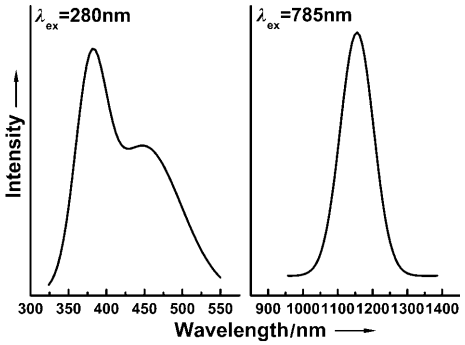

Figure 2. a) UV/blue and b) NIR PL spectra of Ag_2S–ZnS HNSs (Ag(DDTC):$Zn(DDTC)_2$ 2:1) with excitation at 280 and 785 nm, respectively.

centered at 1155 nm with full width at half-maximum (FWHM) of 100 nm was observed in the NIR PL spectrum of Ag_2S in HNSs under 785 nm excitation. This is the first observation of coexisting UV/blue and NIR PL emissions in semiconductor–semiconductor HNSs while keeping their intact nature. However, we noticed that the PL properties of Ag_2S in the as-prepared Ag_2S–ZnS HNSs were different from our recent report[23] in terms of PL emission peak position and the FWHM of the PL spectrum. The Ag_2S QDs, which were synthesized by pyrolysis of Ag(DDTC) in a mixture of oleic acid (OA), octadecylamine (ODA), and 1-octadecane (ODE), have an emission peak at 1058 nm with an extraordinarily narrow FWHM of 21 nm and OA and ODA as surface-capping ligands.[23] Instead, the Ag_2S–ZnS HNSs were obtained through thermal co-decomposition of Ag(DDTC) and $Zn(DDTC)_2$ in a mixture of oleylamine (OM) and 1-dodecanethiol (DT) and are exclusively coated with DT molecules (see Supporting Information). In addition, we observed that the NIR PL intensity of Ag_2S QDs is much lower than that of Ag_2S–ZnS HNSs. We speculated that DT plays a key role in determining the optical properties of Ag_2S, and may be involved in the reaction as a partial sulfur source rather than a mere capping ligand. The exact understanding of this mechanism is still under investigation.

The size of matchstick-shaped Ag_2S–ZnS HNSs could be conveniently tuned by changing the molar ratio of Ag(DDTC) and $Zn(DDTC)_2$, which is impossible for the seeded-growth method with given seeds. When the molar ratio of Ag(DDTC) and $Zn(DDTC)_2$ was decreased to 1:2, uniform Ag_2S–ZnS HNSs consisting of approximately 8.5 nm Ag_2S QDs and approximately 7.8×35 nm ZnS nanorods were obtained (Figure 3a and b; see Supporting Information for detailed characterization). Figure 3c shows the influence of the size on the optical properties of Ag_2S–ZnS HNSs. The ZnS PL peak center was redshifted from 380 to 450 nm and the PL intensity in the UV/blue region was severely diminished when the ZnS nanorod diameter increased from 4 to 7.8 nm, owing to the weakened quantum confinement effect of ZnS (Bohr radius of ZnS: 2.4 nm),[29] in spite of shortening of the length of the ZnS nanorods from 48 to 35 nm. These results were supported by the redshifted absorbance spectra (see Supporting Information) of the two types of Ag_2S–ZnS HNSs in the UV/blue region, as well as

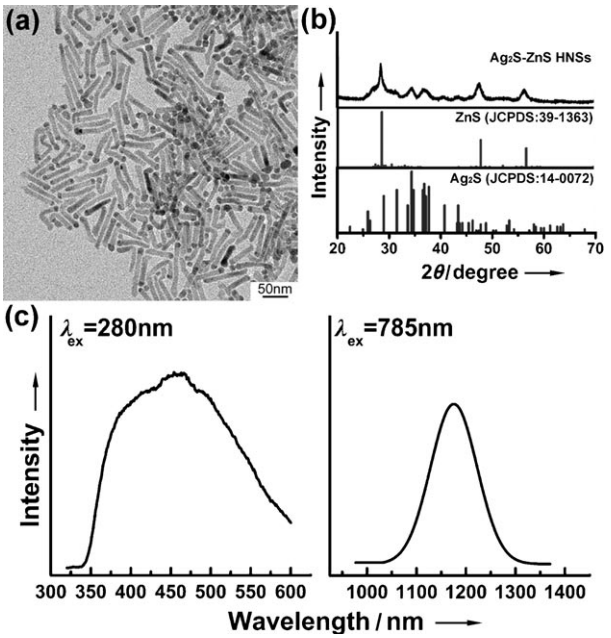

Figure 3. TEM image (a), XRD pattern (b), and UV/blue and NIR PL spectra (c) of Ag_2S–ZnS HNSs with Ag(DDTC):$Zn(DDTC)_2$ 1:2.

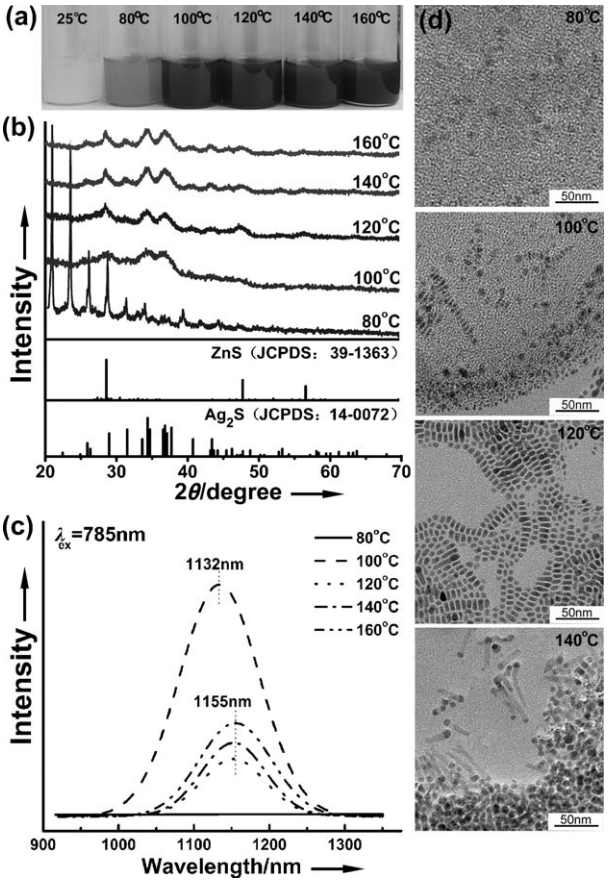

Figure 4. Evolution of Ag_2S–ZnS HNSs with temperature, monitored by a) naked-eye pictures, b) XRD patterns, c) NIR PL spectra, and d) TEM images.

previous reports that the quantum confinement effect of semiconductor CdSe nanorods and ZnS nanorods is mainly determined by lateral rather than longitudinal confinement.[27,30,31] The Ag_2S PL intensity also decreased sharply and was accompanied by an approximately 20 nm redshift, from 1155 to 1175 nm, when the diameter of Ag_2S head in Ag_2S–ZnS HNSs increased from about 4.5 to 8.5 nm, which also could be attributed to the weakened quantum confinement effect resulting from the increase in Ag_2S QD size.

The extensively studied growth mechanism of HNSs through wet chemistry was concluded to be seeded and catalyst-assisted growth.[25] In contrast, we used a one-pot method to obtain the HNSs by thermal codecomposition of two single-source precursors, that is, a significant variation from the literature methods.[1–15,25] Hence, it was of importance to investigate the growth process and formation mechanism of our Ag_2S–ZnS HNSs. During the synthesis, we observed continuous change of the color of the reaction mixture with increasing temperature from 80 to 160 °C (Figure 4a). To understand the formation mechanism of Ag_2S–ZnS HNSs, the growth process was dynamically monitored with XRD, NIR PL spectroscopy, and TEM. The XRD and TEM results (Figure 4b and d) unambiguously illustrated the following process: 1) Neither Ag_2S nor ZnS was produced at 80 °C, because there were no characteristic diffraction peaks or observable nanocrystals. 2) Massive Ag_2S nanocrystals were formed, as their diffraction peaks were clearly indexed, and a small amount of ZnS were also formed, as its characteristic peak appeared in low intensity. The XRD data were consistent with the TEM result that the broadened diffraction peaks were caused by the smaller sizes of the newly generated nanocrystals. The higher peak intensities of Ag_2S indicated initial decomposition of Ag(DDTC) into Ag_2S nuclei accompanied by a few ZnS nuclei from $Zn(DDTC)_2$ at 100 °C. 3) Ag_2S–ZnS HNSs kept growing with increasing temperature up to 120 °C, as the (008) peaks of ZnS became more evident, suggesting anisotropic growth of ZnS nanorods along the (001) direction after selective anchoring of their nuclei on the surface of Ag_2S nuclei. In TEM images this anisotropic growth was revealed by the change in shape of the Ag_2S–ZnS HNSs from nanoparticle to nanorod. 4) ZnS nanorods grew longer and matchstick-shaped Ag_2S–ZnS HNSs formed at elevated temperatures of 140 and 160 °C. Figure 4c shows the changes in NIR PL spectra at different temperatures. There was no PL at 80 °C without formation of Ag_2S. The PL intensity became saturated at 100 °C and then did not change much with increasing temperature. It is noteworthy that a 22 nm redshift and a sharp drop in Ag_2S emission occurred after formation of Ag_2S–ZnS HNSs (120 °C), which may result from the conjunction interface of Ag_2S and ZnS nanocrystals. The mild increase in Ag_2S PL intensity at higher temperatures is presumably attributable to reconstruction of the Ag_2S–ZnS interface during the ripening process.

In summary, we have synthesized well-defined matchstick-shaped Ag_2S–ZnS HNSs using a facile one-pot method involving thermal co-decomposition of single-source precursors Ag(DDTC) and $Zn(DDTC)_2$ in oleylamine/1-dodecanethiol. The size of the Ag_2S–ZnS HNSs can be easily tuned by

changing the reaction conditions. The Ag_2S–ZnS HNSs exhibit appealing PL in both UV/blue and NIR regions. With increasing size of the Ag_2S–ZnS HNSs, PL in both UV/blue and NIR regions shows a significant quantum size effect with decreased PL intensity and redshifted PL peaks. The good crystallinity of Ag_2S and ZnS and the conjunction interface with few defects also make an important contribution to achieving desirable optical properties of Ag_2S–ZnS HNSs. The prepared Ag_2S–ZnS HNSs will provide numerous opportunities for potential applications, such as simultaneous in vitro/in vivo bioimaging and optoelectronic devices. The synthetic method reported here offers a facile approach for precise control of complex HNSs on the nanometer scale.

Received: February 13, 2011
Revised: April 27, 2011
Published online: June 21, 2011

Keywords: heterostructures · luminescence · nanostructures · quantum dots · semiconductors

[1] T. Mokari, E. Rothenberg, I. Popov, R. Costi, U. Banin, *Science* **2004**, *304*, 1787.
[2] P. D. Cozzoli, T. Pellegrino, L. Manna, *Chem. Soc. Rev.* **2006**, *35*, 1195.
[3] T. Pellegrino, A. Fiore, E. Carlino, C. Giannini, P. D. Cozzoli, G. Ciccarella, M. Respaud, L. Palmirotta, R. Cingolani, L. Manna, *J. Am. Chem. Soc.* **2006**, *128*, 6690.
[4] W. L. Shi, H. Zeng, Y. Sahoo, T. Y. Ohulchanskyy, Y. Ding, Z. L. Wang, M. Swihart, P. N. Prasad, *Nano Lett.* **2006**, *6*, 875.
[5] H. Yu, M. Chen, P. M. Rice, S. X. Wang, R. L. White, S. H. Sun, *Nano Lett.* **2005**, *5*, 379.
[6] J. Yang, H. I. Elim, Q. Zhang, J. Y. Lee, W. Ji, *J. Am. Chem. Soc.* **2006**, *128*, 11921.
[7] H. Gu, Z. Yang, J. Gao, C. K. Chang, B. Xu, *J. Am. Chem. Soc.* **2005**, *127*, 34.
[8] J. Jiang, H. W. Gu, H. L. Shao, E. Devlin, G. C. Papaefthymiou, J. Y. Ying, *Adv. Mater.* **2008**, *20*, 4403.
[9] S. E. Habas, H. Lee, V. Radmilovic, G. A. Somorjai, P. D. Yang, *Nat. Mater.* **2007**, *6*, 692.
[10] M. Pang, J. Hu, H. C. Zeng, *J. Am. Chem. Soc.* **2010**, *132*, 10771.
[11] T. Mokari, C. G. Sztrum, A. Salant, E. Rabani, U. Banin, *Nat. Mater.* **2005**, *4*, 855.
[12] A. Salant, E. Amitay-Sadovsky, U. Banin, *J. Am. Chem. Soc.* **2006**, *128*, 10006.
[13] S. E. Habas, P. D. Yang, T. Mokari, *J. Am. Chem. Soc.* **2008**, *130*, 3294.
[14] J. Maynadié, A. Salant, A. Falqui, M. Respaud, E. Shaviv, U. Banin, K. Soulantica, B. Chaudret, *Angew. Chem.* **2009**, *121*, 1846; *Angew. Chem. Int. Ed.* **2009**, *48*, 1814.
[15] S. Deka, A. Falqui, G. Bertoni, C. Sangregorio, G. Poneti, G. Morello, M. De Giorgi, C. Giannini, R. Cingolani, L. Manna, P. D. Cozzoli, *J. Am. Chem. Soc.* **2009**, *131*, 12817.
[16] V. Subramanian, E. E. Wolf, P. V. Kamat, *J. Am. Chem. Soc.* **2004**, *126*, 4943.
[17] W. T. Chen, T. T. Yang, Y. J. Hsu, *Chem. Mater.* **2008**, *20*, 7204.
[18] R. Costi, G. Cohen, A. Salant, E. Rabani, U. Banin, *Nano Lett.* **2009**, *9*, 2031.
[19] D. V. Talapin, R. Koeppe, S. Gotzinger, A. Kornowski, J. M. Lupton, A. L. Rogach, O. Benson, J. Feldmann, H. Weller, *Nano Lett.* **2003**, *3*, 1677.
[20] A. Dong, R. Tang, W. E. Buhro, *J. Am. Chem. Soc.* **2007**, *129*, 12254.
[21] R. D. Robinson, B. Sadtler, D. O. Dechenko, C. K. Erdonmez, L. W. Wang, A. P. Alivisatos, *Science* **2007**, *317*, 355.
[22] H. McDaniel, J. M. Zuo, M. Shim, *J. Am. Chem. Soc.* **2010**, *132*, 3286.
[23] Y. Du, B. Xu, T. Fu, M. Cai, F. Li, Y. Zhang, Q. B. Wang, *J. Am. Chem. Soc.* **2010**, *132*, 1470.
[24] Y. Zhang, H. Xu, Q. B. Wang, *Chem. Commun.* **2010**, *46*, 8941.
[25] G. Zhu, Z. Xu, *J. Am. Chem. Soc.* **2011**, *133*, 148.
[26] K. An, N. Lee, J. Park, S. C. Kim, Y. Hwang, J. G. Park, J. Y. Kim, J. H. Park, M. J. Han, J. Yu, T. Hyeon, *J. Am. Chem. Soc.* **2006**, *128*, 9753.
[27] J. H. Yu, J. Joo, H. M. Park, S. I. Baik, Y. W. Kim, S. C. Kim, T. Hyeon, *J. Am. Chem. Soc.* **2005**, *127*, 5662.
[28] S. Wageh, Z. S. Ling, X. Xu-Rong, *J. Cryst. Growth* **2003**, *255*, 332.
[29] Q. B. Wang, D.-K. Seo, *Chem. Mater.* **2006**, *18*, 5764.
[30] J. Hu, L. S. Li, W. Yang, L. Manna, L. W. Wang, A. P. Alivisatos, *Science* **2001**, *292*, 2060.
[31] L. S. Li, J. Hu, W. Yang, A. P. Alivisatos, *Nano Lett.* **2001**, *1*, 349.

